

Qing Trepte
*Science Applications International Corporation
Hampton, VA*

Patrick Minnis
NASA Langley Research Center, Hampton, VA

Rabindra Palikonda and Doug Spangenberg
*Analytical Services and Materials, Inc.
Hampton, Virginia*

Martial Haeffelin
Lab. de Meteorologie Dyn., IPSL, Palaiseau, France

1. Introduction

Thin cirrus clouds account for about 20-30% of the total cloud coverage and affect the global radiation budget by increasing the Earth's albedo and reducing infrared emissions. Thin cirrus, however, are often underestimated by traditional satellite cloud detection algorithms. This difficulty is caused by the lack of spectral contrast between optically thin cirrus and the surface in techniques that use visible (0.65 μm) and infrared (11 μm) channels.

In the Clouds and the Earth's Radiant Energy System (CERES) *Aqua* Edition 1 (AEd1) and *Terra* Edition 3 (TEd3) Cloud Masks, thin cirrus detection is significantly improved over both land and ocean using a technique that combines MODIS high-resolution measurements from the 1.38 and 11 μm channels and brightness temperature differences (BTDs) of 11-12, 8.5-11, and 3.7-11 μm channels. To account for humidity and view angle dependencies, empirical relationships were derived with observations from the 1.38 μm reflectance and the 11-12 and 8.5-11 μm BTDs using 70 granules of MODIS data in 2002 and 2003.

Another challenge in global cloud detection algorithms occurs near the day/night terminator where information from the visible 0.65 μm channel and the estimated solar component of 3.7 μm channel becomes less reliable. As a result, clouds are often underestimated or misidentified near the terminator over land and ocean.

Comparisons between the CLAVR-x (Clouds from Advanced Very High Resolution Radiometer [AVHRR]) cloud coverage and Geoscience Laser Altimeter System (GLAS) measurements north of 60°N indicate significant amounts of missing clouds from CLAVR-x because this part of the world was near the day/night terminator viewed by AVHRR. Comparisons between MODIS cloud products (MOD06) and GLAS in the same region also show similar difficulties with MODIS cloud retrievals (Pavolonis, 2005). The consistent detection of clouds through out the day is needed to provide reliable cloud

and radiation products for CERES and other research efforts involving the modeling of clouds and their interaction with the radiation budget.

The twilight cloud detection algorithms in the CERES cloud mask have been improved using both MODIS and Geostationary Operational Environmental Satellite (GOES) data. Because *Terra* and *Aqua* are polar-orbiting satellites, MODIS sees twilight regions mostly at high latitudes and often over snow surfaces. An improved twilight algorithm utilizes MODIS 2-km multi-spectral measurements: visible 0.65 and 1.6 μm (2.1 μm for *Aqua*) reflectances, 11 μm brightness temperatures, and the 3.7-11 and 6.7-11 μm BTDs to differentiate between clouds and snow surfaces. With the TE3d cloud mask, the MODIS derived global cloud fraction shows a smoother transition from the midlatitudes into polar regions.

Unlike polar orbiting satellites, geostationary satellites (GOES 10 and 12) provide continuous temporal sampling over low and midlatitudes and a good opportunity to examine how cloud detection/retrieval algorithms work at all local times. The GOES cloud detection algorithm is based on the CERES TEd2 cloud mask. Because of spectral differences between GOES and MODIS, threshold adjustments have been made for application to the ARM (Atmosphere Radiation Measurement) GOES measurements. This adjusted cloud mask algorithm is designated the CERES ARM Cloud Mask (CACM). The original version of the CACM is V1.1. The improved version is called V2.1. It is used for real-time GOES cloud retrievals (Minnis et al., 2004) over the continental United States (CONUS) and environs (55°N-20°S and 130°W-65°W). The GOES cloud detection algorithm utilizes the 4-km GOES VIS reflectance, 10.8- μm brightness temperatures, and the BTDs for 3.9-11 μm and 6.7-10.8 μm , 10.8-13 μm (for GOES-12), and 10.8-12 μm (for GOES-10), together with the predicted background clear-sky information to detect various types of clouds and snow (in winter seasons). The results show improvement in cloud amount over the ARM Southern Great Plains (SGP) site. The improved near-terminator is validated using Micropulse Lidar (MPL) observations and the Millimeter-Wavelength Cloud Radar (MMCR) measurements at SGP site.

*Corresponding author address: Q. Trepte, SAIC, 1 Enterprise Pkwy., Suite 300, Hampton, VA 23666
email: q.z.trepte@larc.nasa.gov

2. Data and Methodology

This study uses Terra and Aqua MODIS and GOES-10, and 12 radiance measurements. The ancillary data used here include the atmospheric profiles and surface skin temperature: Goddard Modeling and Assimilation Office (GMAO) data for CERES operational, hourly Rapid Update Cycle (RUC; Benjamin et al., 2004) sounding data over U.S. for GOSE processing, daily snow and ice maps from the NOAA Satellite Services Division (SSD); 10' surface emissivity maps at 3.9 and 11 μm derived from MODIS data (Chen et al. 2004); CERES clear-sky VIS reflectance maps derived from MODIS (Sun-Mack et al., 2003); IGBP (International Geosphere Biosphere Program) ecosystem map; water percentage and surface elevation maps.

The CERES cloud mask is used as the scene identification method for the operational CERES products (Trepte et al., 1999). The technique is based primarily on a cascade of threshold tests utilizing the radiances taken at 0.65, 3.9, 6.5, 11, and 12.0 or 13.3 μm compared with the predicted clear-sky 0.65- μm reflectance, 11- μm top-of-atmosphere (TOA) T_{11} , and TOA $T_{3.7}-T_{11}$. Clear-sky albedo maps, directional and bidirectional reflectance models (Sun-Mack et al., 2004) are used to predict the expected clear-sky reflectances. Clear-sky TOA brightness temperatures T_{cs} are estimated from surface skin temperature for 3.7, 10.8 and 12- μm channels using the surface emissivities and computing the atmospheric effects on the upwelling radiance using temperature and humidity profiles. The clear-sky maps are resolved to 10' of latitude and longitude. Thresholds are based on spatial and temporal variation within a 10" box. The scenes are classified as clear or cloudy with additional subcategories. Clear categories include strong, weak, smoke, fire, snow, sun-glint, shadow, and aerosol. Cloudy classifications include strong, weak, sun-glint. The strong and weak refer to the certainty of the classification.

2.1 CERES-MODIS daytime thin cirrus detection

Surface validation using ground-based lidar at SIRTa, France (Chiriaco et al. 2005), shows that the Terra Edition 2 (TEd2) CERES cloud mask underestimates thin ice clouds over land. In TEd2, the traditional visible channels, 0.65 and 1.6 μm , together with IR channels were used to detect various clouds. For very thin cirrus, the reflectances from 0.65 and 1.6 μm have little contrast compared with their background clear sky values. In the AEd1 cloud mask (CERES operational since 2004) and the TEd3 cloud mask (planned operational start date in late 2006), a new daytime thin cirrus detection algorithm was developed using MODIS 1.38- μm reflectance ($\rho_{1.38}$), together with the 3.75–11, 11–12, and 8.5–11 μm BTDs. Since $\rho_{1.38}$, $T_{11}-T_{12}$, and $T_{8.5}-T_{11}$ vary with water vapor loading in the atmosphere and satellite view angles, empirical relations of $\rho_{1.38}$, $T_{11}-T_{12}$, and $T_{8.5}-T_{11}$ as functions of atmospheric column precipitable water (PW) and view angles (VZA) were developed. The study was based on

70 5-minute granules of MODIS data over various land and desert surfaces and PW was calculated from GMAO profiles. It was found that the VZA dependency of $\rho_{1.38}$ and $T_{8.5}-T_{11}$ was less significant than the PW dependency; thus, these dependencies are not considered further. Figure 1 displays the polynomial fits of $\rho_{1.38_PW}$, $T_{11}-T_{12_PW}$, and $T_{8.5}-T_{11_PW}$ as functions of PW for clear-sky conditions.

The daytime thin cirrus tests over land and desert are:

1. $r_{1.38} > (r_{1.38_PW} + 0.002)$
2. For land: $T_{11} - T_{12} > T_{11cs} - T_{12cs} - 0.5$
or $T_{11} - T_{12} > Ci_thr$
For desert: $T_{11} - T_{12} > T_{11} - T_{12_PW}$
or $T_{11} - T_{12} > Ci_thr$
3. $T_{8.5} - T_{11} > T_{8.5} - T_{11_PW} + 1$
4. $T_{3.7} - T_{11} > (T_{3.7cs} - T_{11cs}) + 1$

where $T_{3.7cs}$, T_{11cs} and T_{12cs} are predicted clear sky TOA temperatures and Ci_thr is the T_{11} and VZA dependent thresholds. If a pixel passes all four tests, it is classified as cloudy.

Over ocean, a pixel is classified as cloudy when

$$\begin{aligned} T_{cs11} - T_{11} &> 2.5 \text{ K} \\ r_{1.38} &> 0.008 \\ T_{11} - T_{12} &> Ci_thr \\ T_{11} - T_{12} &> T_{cs11} - T_{cs12}. \end{aligned}$$

These tests are not sensitive to sun glint over ocean. The $T_{cs11}-T_{11} > 2.5 \text{ K}$ test sometimes prevents detection of very thin cirrus due to its very weak IR signature.

2.2 GOES twilight cloud detection

In previous CACMV1.1 analyses, it was found that as the sun approaches the day/night terminator (solar zenith angle, SZA $> 70^\circ$), the CACMV1.1 mask missed stratus clouds off the California coast and sometimes over the central CONUS. In the "twilight zone" ($82^\circ < \text{SZA} < 87.5^\circ$), "clear bands" often crossed the continental U.S.. Several improvements have been made based on evaluations of the CACMV1.1 cloud mask to correct these problems. The newer CACM version, V2.1 developed here, uses VIS reflectance, together with the IR channels and the snow map as outlined below.

A pixel is classified cloudy if,

Over snow-free land:

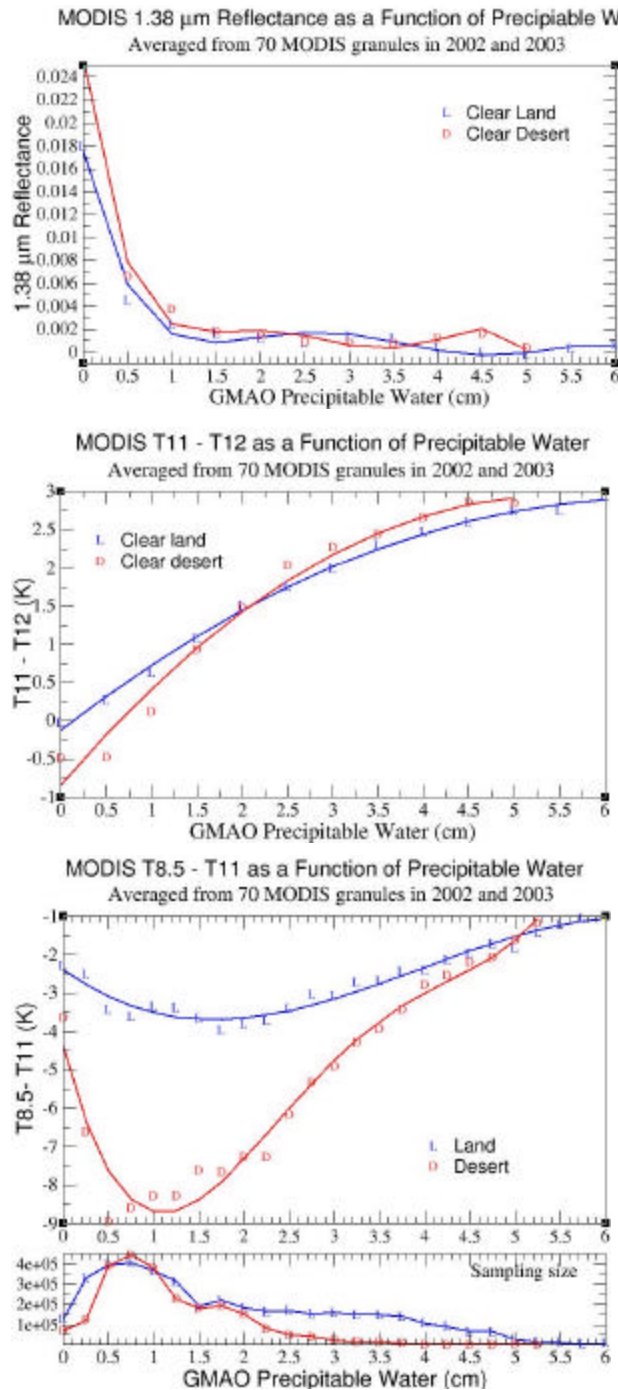


Fig. 1. Functional dependencies of $\rho_{1.38}$, $T_{11}-T_{12}$, and $T_{8.5}-T_{11}$ with precipitable water.

If $r_{0.65} > (r_{cs0.65} + 0.10)$ and
 $((T_{3.9} - T_{11} > 1$ and $T_{cs11} - T_{11})$ or $T_{3.9} - T_{11} < -1)$

Over snow surface:

If $T_{3.9} - T_{11} > (T_{cs3.9} - T_{cs11} + 0.75 * s_{3.9})$ and $T_{cs11} - T_{11} > 0.5 * s_{11}$ and $r_{0.65} > r_{cs0.65} + 0.10$.

Over water:

If $\rho_{0.65} > (\rho_{cs0.65} + 0.05$ and $\rho_{0.65} > 0.20$ and $T_{cs11} - T_{11} > 0$ or $T_{cs11} - T_{11} > 1.5 * s_{11}$.

where $\rho_{0.65}$ is VIS reflectance, CS refers to clear-sky, and ? is the uncertainty in the clear-sky estimate.

Additionally for GOES-12:

$T_{11} - T_{13} < 10$ and $(T_{3.9} - T_{11} > 3$ or $T_{3.9} - T_{11} < -0.5)$.

If no clouds are detected by the above cloud tests, a pixel will be assigned as clear snow, where $T_{skin} < 277$ K and snow map > 0 .

During daytime with high SZAs ($70^\circ < SZA < 82^\circ$), $T_{3.9} - T_{11}$ thresholds were refined to account for the cancellation of $3.9 \mu\text{m}$ reflected solar component in order to detect more low clouds over land and ocean.

2.3 CERES-MODIS twilight polar cloud detection

MODIS sees twilight mostly at high latitudes. The twilight polar cloud tests were developed for CERES TE_{d2} (Trepte, et al, 2002) and further improved in TE_{d3}. In addition to the $0.65\text{-}\mu\text{m}$ visible reflectance, the ratio of 1.6 to $0.65 \mu\text{m}$ (2.1 to 0.65 for Aqua) was also used in MODIS Terra and Aqua twilight algorithms. The theoretical snow reflectance models of 0.65 , 1.6 , $2.1 \mu\text{m}$ were used as clear sky values over snow surfaces.

3. Results

The impact of the changes in the mask are illustrated with the aid of a few examples showing comparisons with the old CERES mask, results from the Collection 4 MOD06 mask (Ackerman et al., 2000), and with objective surface measurements.

3.1 Thin cirrus detection

Figure 2 shows the CERES cloud mask results compared with ground-based lidar measurements at SIRTa observatory (Figure 3) near Palaiseau, France (indicated by a small red box in the middle of the image) on 6 November 2003. The CERES TE_{d3} mask identifies more thin cirrus than with TE_{d2}. Note the cloud layer at 11:40 AM was observed between 10-11 km by the lidar. Figure 4 shows a comparison between the traditional thin cirrus cloud detection in TE_{d2} with the improved algorithm in TE_{d3} at the SIRTa observatory. The upper right panel represents a composite MODIS image of 0.65 , 1.6 , and $3.7\text{-}11 \mu\text{m}$. The TE_{d2} cloud mask and clear categories are shown on the lower portion of the left column and the TE_{d3} results are on the right column. Not only does TE_{d3} identify more clouds, it also detects more snow (red in RGB image) that was previously misidentified as clouds by TE_{d2}.

Figure 5 compares the CERES TE_{d2}, TE_{d3}, and MOD06 cloud masks. CERES TE_{d3} significantly improves thin cirrus detection in comparison with TE_{d2} and MOD06. Both TE_{d2} and MOD06 have similar results. In addition, snow was detected more accurately over the Sierra Nevada by TE_{d3}.

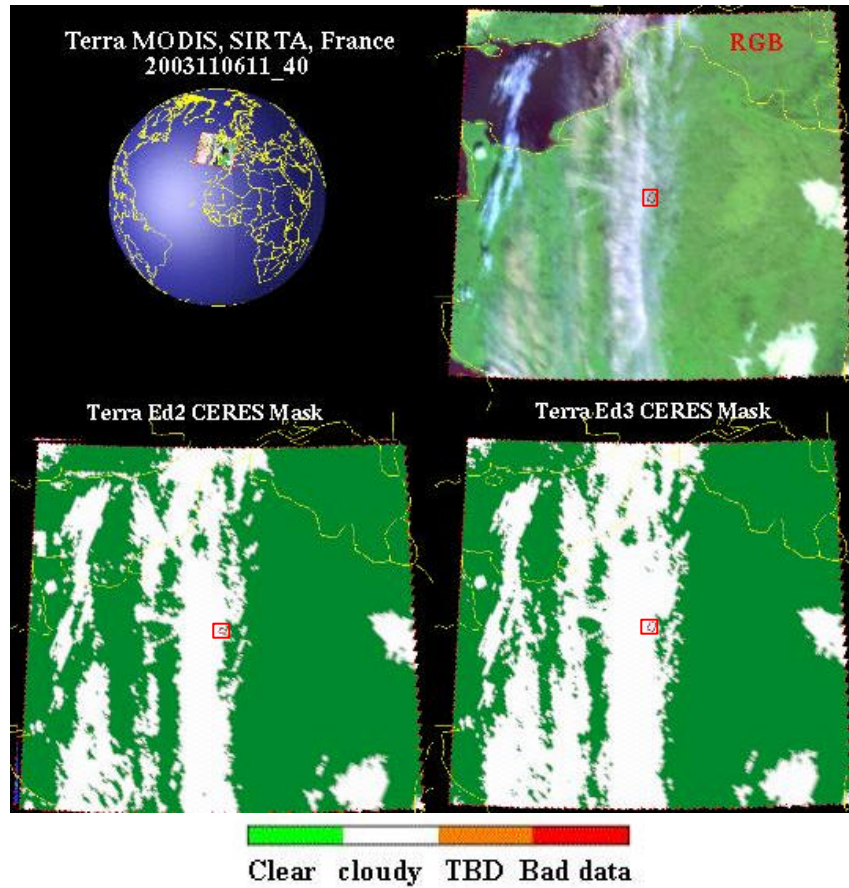


Fig. 2. Terra MODIS, 6 November 2003, 1140 UTC, SIRTA, France. Top right: composite image using 0.65, 1.6, and 3.7-11 μm : Bottom panels: CERES cloud mask TE2 (left) and TE3 (right).

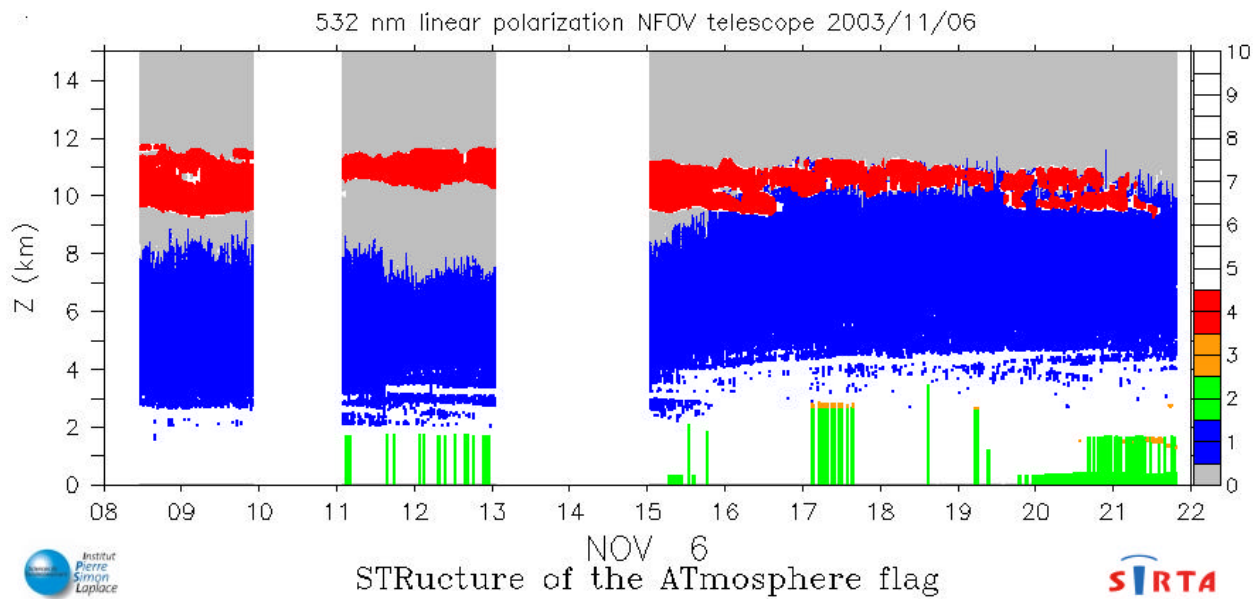


Fig. 3. LNA lidar cloud mask for Nov. 6, 2003, 1140 UTC, at SIRTA observatory. "flag = 0: no significant power return, flag = 1: molecular, flag = 2: boundary layer, flag = 3: aerosol layer, flag = 4: cloud layer, flag = 4: no detection".

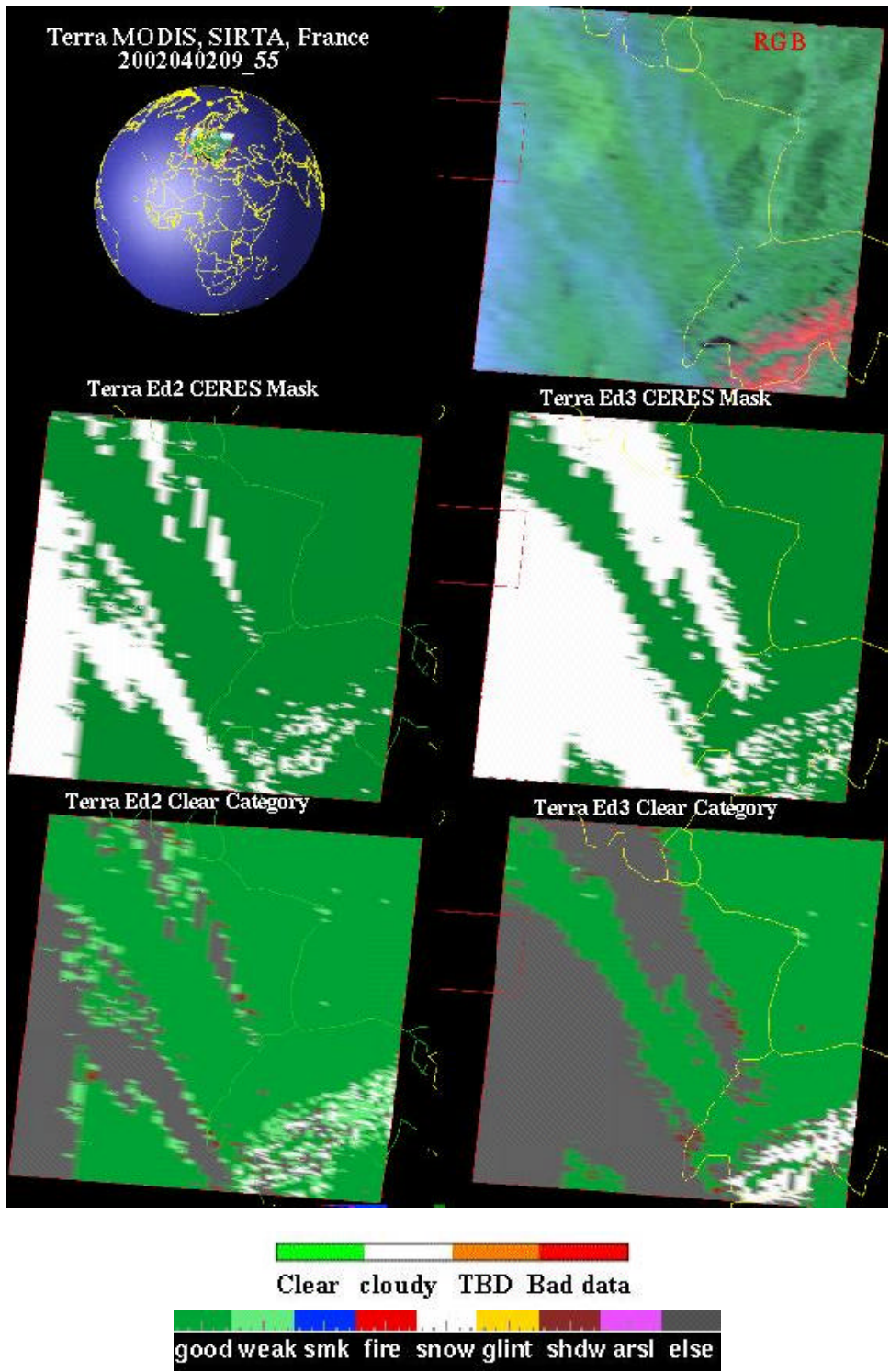


Fig. 4. Terra MODIS imagery. 2 April 2002, 0955 UTC, at the SIRT A observatory in France. The top color bar represents the CERES Cloud Mask and the bottom color bar represents the clear category.

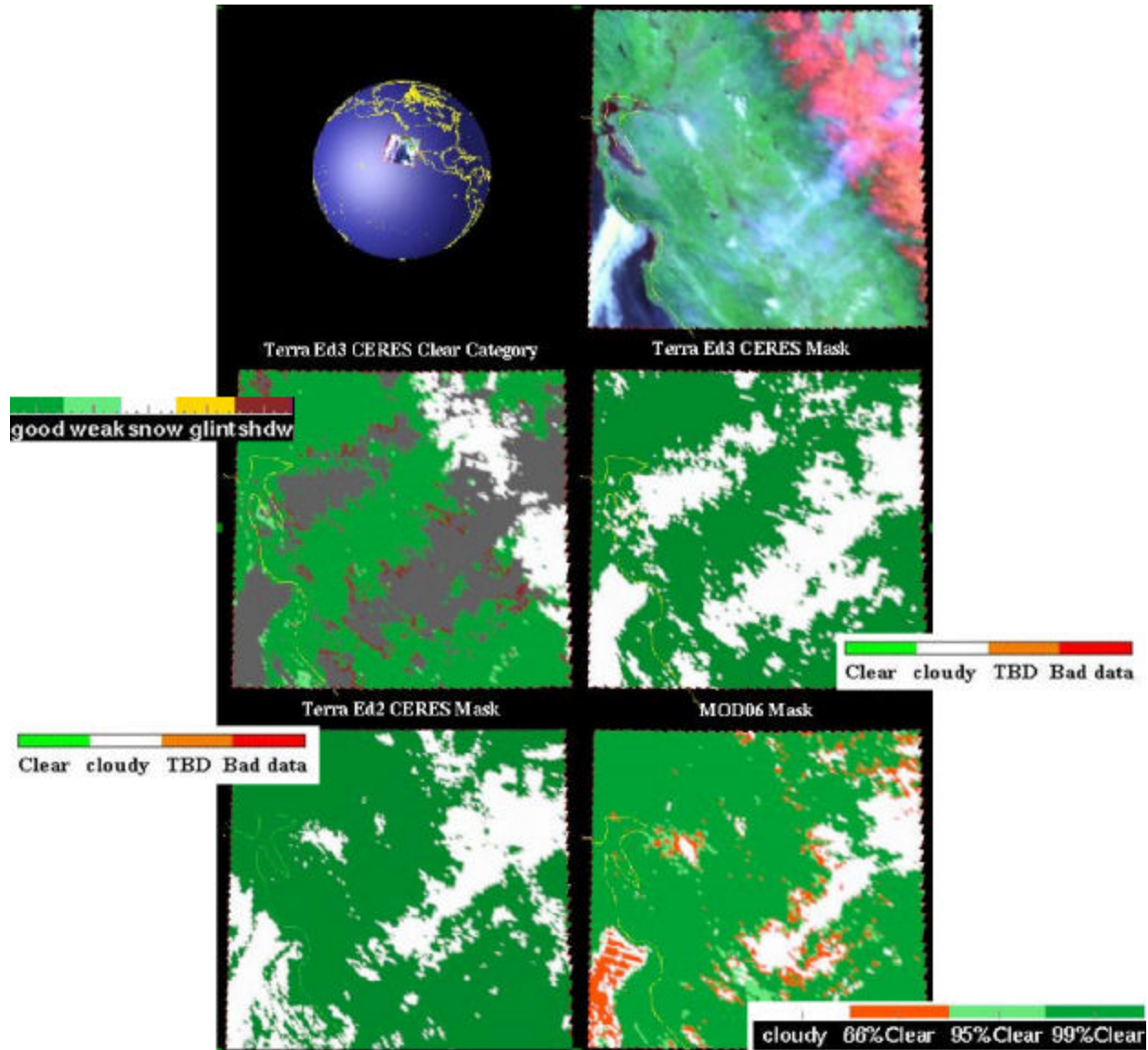


Fig. 5. Terra MODIS imagery, 6 March 2005, 1920 UTC, near San Francisco, California.

An example of improvement in the AEd1 thin cirrus detection is shown in Fig. 6. The thin cirrus off the California coast was completely missed by CERES TE2 (applied to *Aqua* data) and MOD06, but was detected by the CERES AEd1. However, some very thin cirrus was still under-detected by AEd1 due to weak IR signals.

3.2. Improved twilight cloud detection

Figure 7 compares the performance of CACM V1.1 and V2.1 in near-terminator conditions off the California coast. The top two panels are GOES-10 IR and VIS images. The SZAs vary between 65 and 82°. The warm stratus clouds produce very weak signal in IR image,

but are evident in the VIS image. By refining the cloud test for large SZAs, the V2.1 detects the warm status that was missed by V1.1. In this case, the inclusion of more weight for the VIS reflectance thresholds in the decision results in dramatic improvements in the CACM in low sun conditions.

Figure 8 shows a cyclone crossing the midwestern U.S. during the twilight period. The infrared channels-based V1.1 mask missed the warm clouds over the northern plains since the IR signals are small. The new twilight cloud tests, applied when $82^\circ < \text{SZA} < 87.2^\circ$, which use the VIS reflectance together with new 10.8- μm and BTD thresholds to significantly improve the twilight cloud mask, reduced the “clear band” as seen in V1.1 mask.

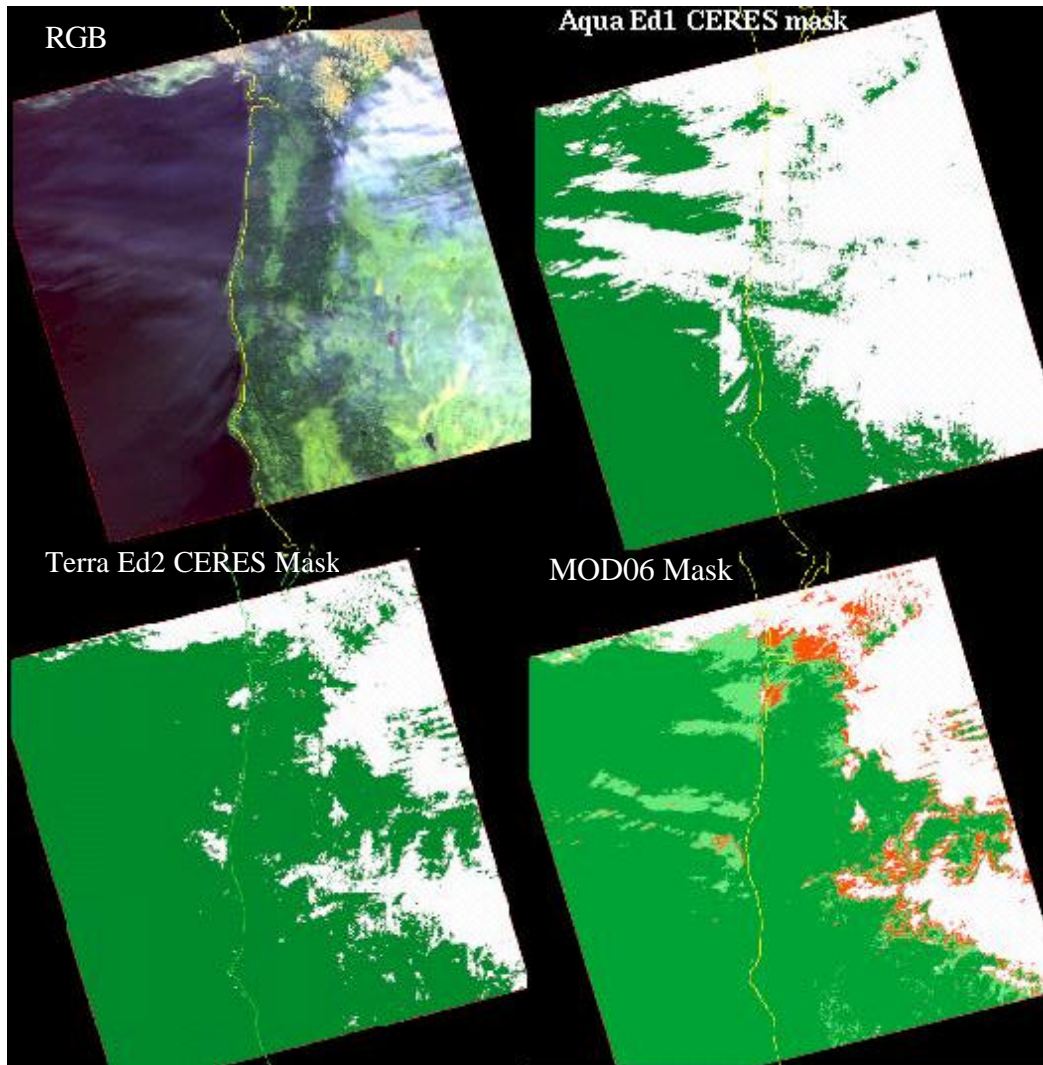


Fig. 6. Aqua MODIS, 27 October , 2003, 2055 UTC, off North California coast. See color bar for Fig. 5.

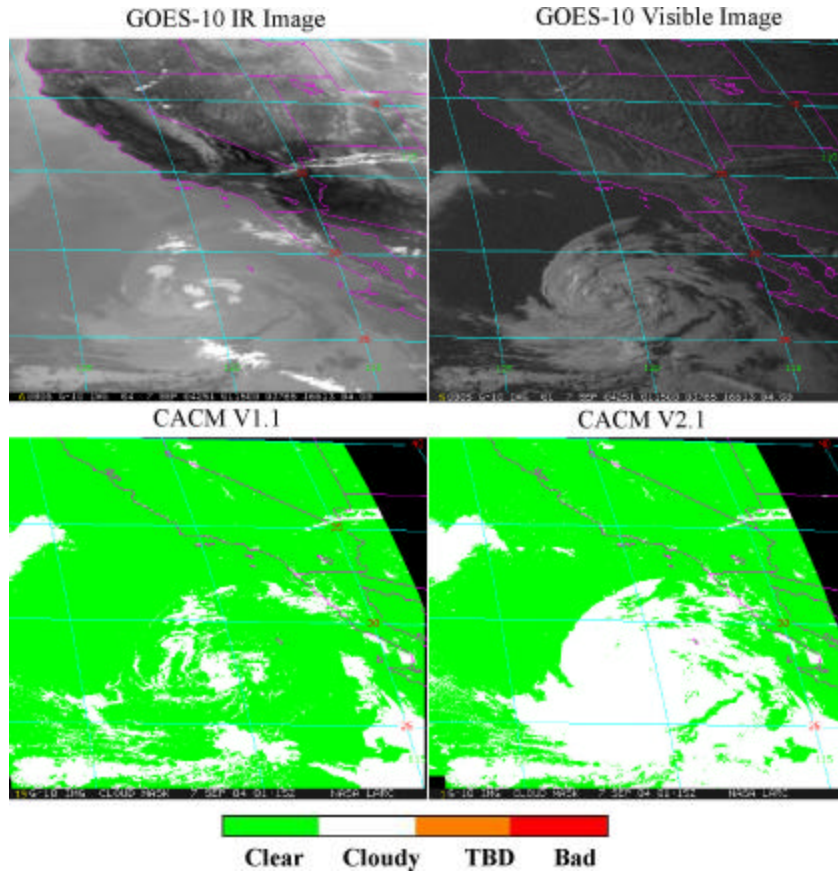


Fig. 7. GOES-10, 7 September 2004, 0115 UTC.

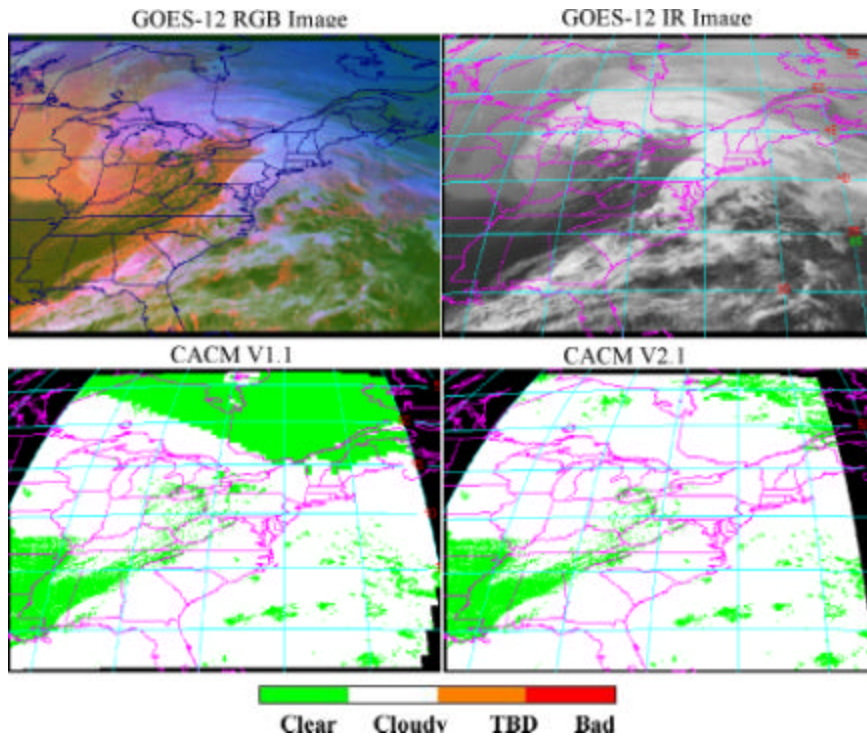


Fig. 8. GOES-12, 7 December 2004, 2015 UTC.

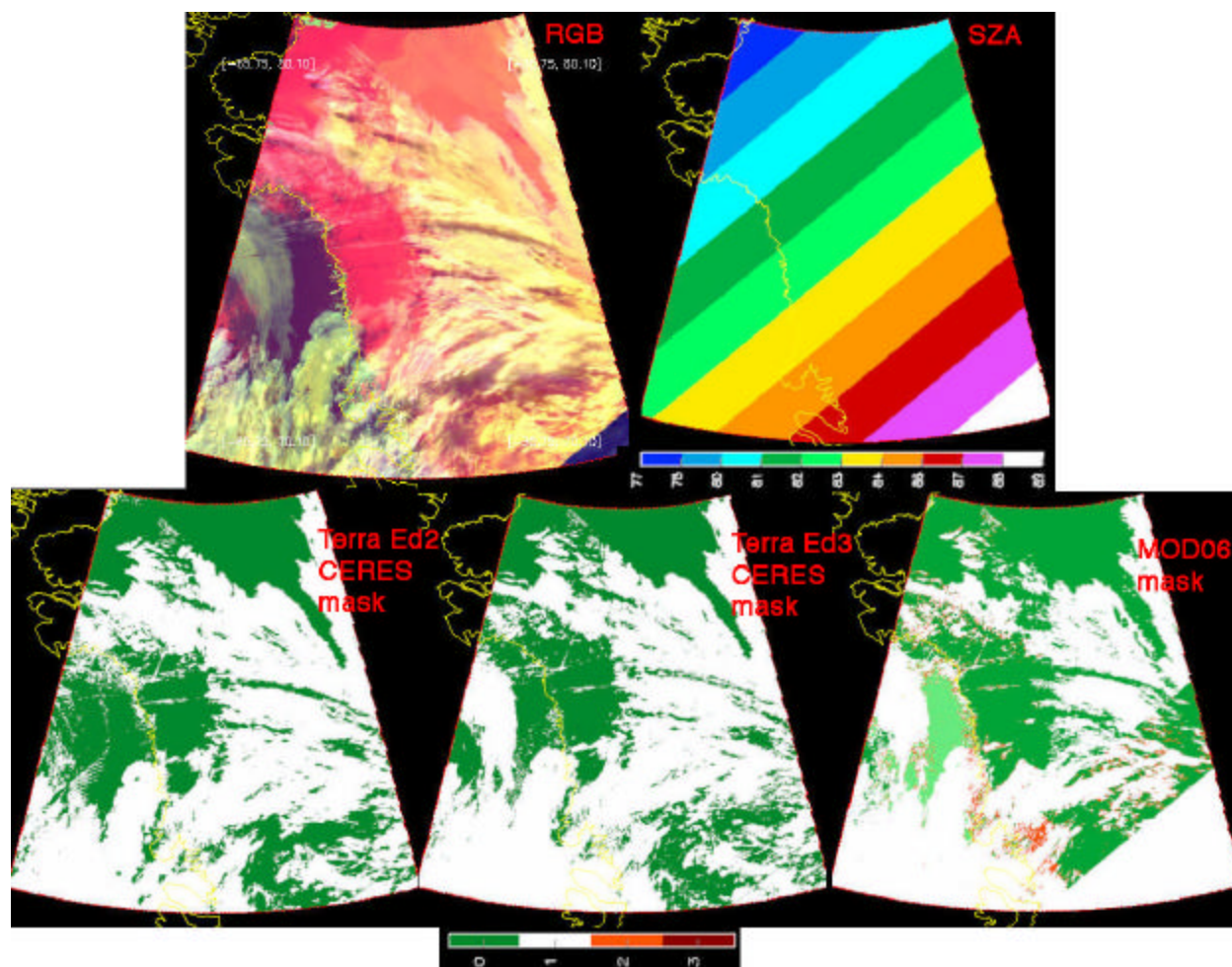


Fig. 9. Terra MODIS, 30 July, 2005, 0040 UTC, Greenland and Baffin Bay. See color bar for Fig. 5.

An example of improvement in twilight low cloud detection for TEd3 compared with TEd2 and MOD06 is shown in Figure 9. The top-left panel is a composite RGB image (0.65, 1.6, 3.7-11 μm) and the SZA ranges from 77 to 89°. TEd3 picked up the low clouds in Baffin Bay that were under-detected by TEd2. The MOD06 mask missed some low cloud over Greenland, and also has striping across day-night terminator, a common problem for global cloud detection algorithms that also affects CERES global cloud fraction in some months.

Figure 10 shows the CERES daytime global cloud fraction for May 2004. In early summer at high northern latitudes, Sun angles are often low. Discontinuities are sometimes found for latitudes between 50 to 60°N. This example shows a discontinuity line crossing Siberia in TEd2 (top plot with arrow). In AEd1 (bottom plot), the discontinuity at the same location was improved. However, in some months, CERES AEd1 daytime and nighttime global cloud fraction plots still have discontinuity lines which needs further improvements.

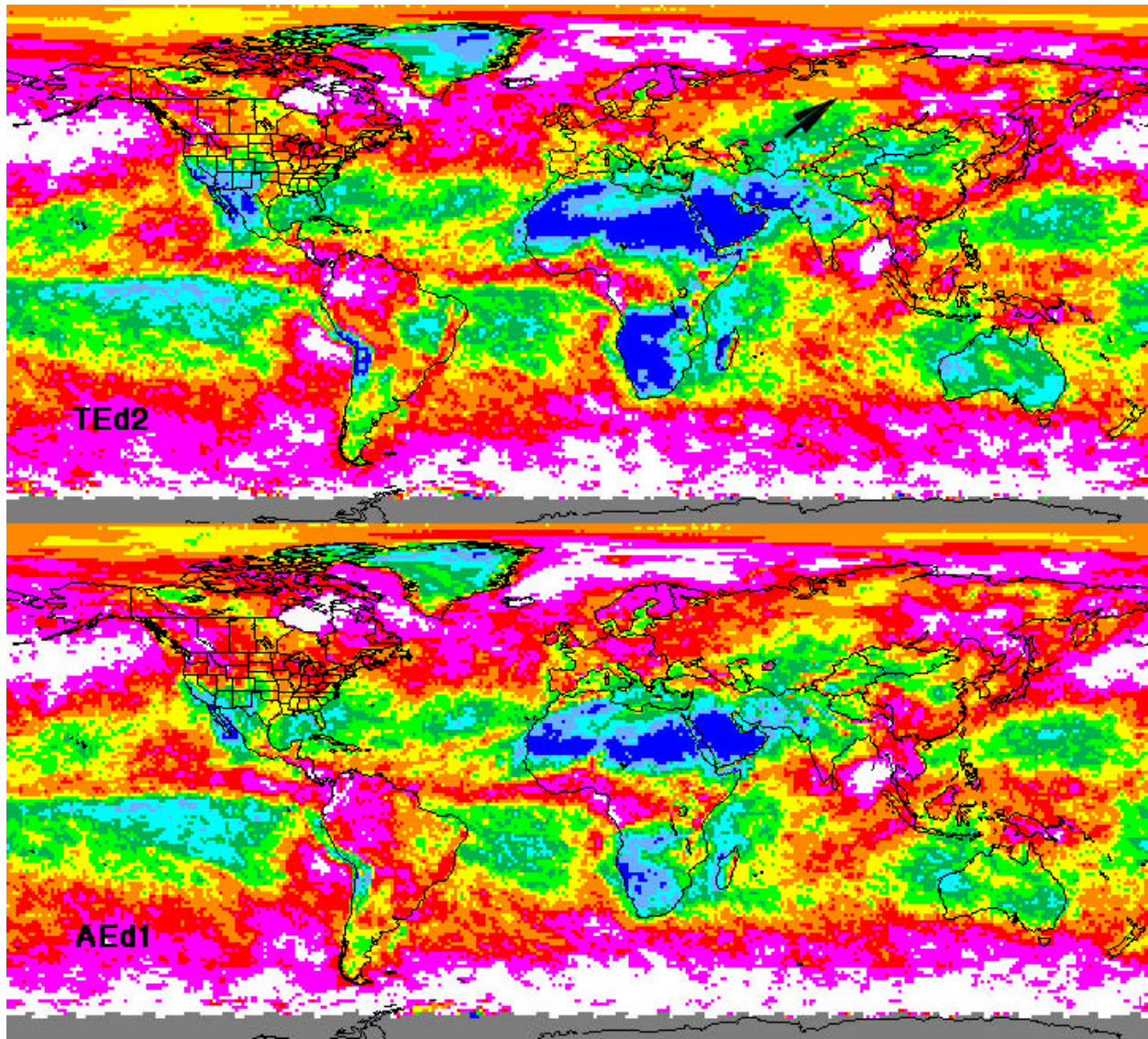


Fig. 10. Daytime monthly global cloud fraction for May 2004, top: CERES TEd2; bottom: CERES AEd1.

3.3. Validation at SGP site

The CACM V1.1 and V2.1 cloud fractions for 31 January and 20 February 2005 were compared with cloud detections at the ARM Southern Great Plains (SGP) Central Facility. The results are shown in Fig. 11. The mean CACM retrieved cloud amount was calculated for a 20-km x 20-km box centered at SGP using GOES-10 data. Micropulse Lidar (MPL) measurements at SGP site are also plotted for the same time period.

At local twilight and during nighttime (00 - 14 UTC), the V2.1 cloud mask increases the cloud amount by 10-90% on 31 January and by roughly 50% on 20 February with some exceptions. The MPL indicates that the cloud cover is relatively heavy throughout the day on the 31st, but around 1345 UTC (twilight) in Fig. 11 the V2.1 cloud fraction drops to 0.2 and returns to overcast in the next image. Except for this anomaly, the observations match

well with the cloudy and clear portions throughout 31 January. The agreement is relatively good at night on the 20th (Fig. 12), but not during daytime. The cloud height is extremely variable, even extending up to 20 km suggesting the cloud heights are interpreted from noise in the MPL returns. In Fig. 13, the SGP MMCR reflectivity imagery and GOES-10 RGB imagery at four different times show clear skies over the SGP during the daytime (14 - 20 UTC) on 20 February 2005, which agrees well with the V2.1 results. Most of the newly detected clouds from V2.1 are at very low altitudes.

4. Conclusions and Future Work

The TEd3 and AEd1 CERES cloud mask improved the thin cirrus cloud detection over both land and ocean using *Terra* and *Aqua* MODIS 1.38 μm , and other visible and IR channels. The GOES CACM V2.1 cloud mask

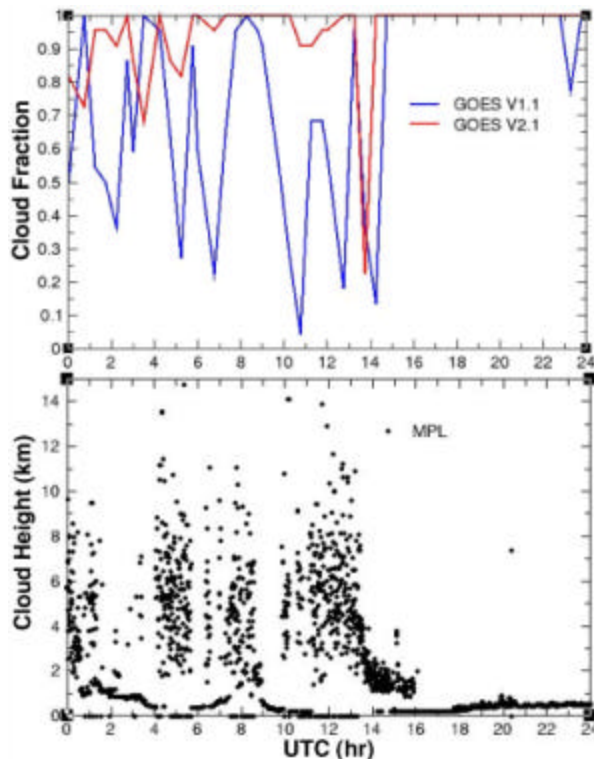


Fig. 11. Top: Comparison of cloud fraction at SGP site between CACM V1.1 and V2.1, 31 January 2005; Bottom: MPL measurements of cloud heights.

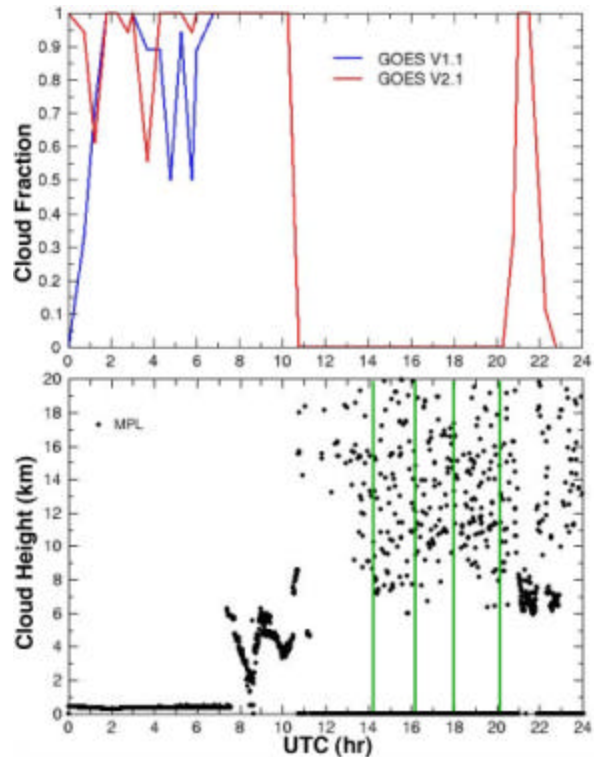


Fig. 12. Top: Comparison of cloud fraction at SGP site between CACM V1.1 and V2.1, 20 February, 2005. Bottom: MPL measurements of cloud heights.

improved the cloud detection near the day/night terminator where the observed $T_{3.7} - T_{11}$ signals are weak due to cancellation of the reflected solar component of $3.9 \mu\text{m}$ and the lack of contrast in the $11\text{-}\mu\text{m}$ channel for warm low clouds. Twilight cloud tests, which utilize the GOES visible and IR channels, smooth the transition between daytime and nighttime cloud retrievals. The cloud fraction from the improved GOES cloud mask agrees well with surface measurements from MPL and MMCR data at ARM SGP site. MODIS twilight polar improvements in AEd1 and TEd3 reduced the discontinuities at day/night terminator and smoothed the transition between mid and high latitudes.

Additional enhancements are needed for the CERES and GOES cloud masks over snow-covered mountains, shadows of high-over-low clouds, dust over desert and ocean, smoke over the Gulf of Mexico, and clouds over bright desert regions. More accurate estimates of clear sky visible, skin temperature, and surface emissivity are also necessary for further gains in cloud detection accuracy, especially at night. These future changes in the cloud mask will be intensely scrutinized with observations at all of the ARM surface sites.

Acknowledgements

This research was supported by the NASA Science Mission through the CERES Project and by the Environmental Sciences Division of the U.S. Department of Energy Interagency Agreement DE-AI02-97ER62341 under the ARM Program.

References

- Ackerman, S. A., K. I. Strabala, W. P. Menzel, R. A. Frey, C. C. Moeller, and L. E. Gumley, 1998: Discriminating clear sky from clouds with MODIS. *J. Geophys. Res.*, **103**, 32141-32157.
- Benjamin, S. G., and Coauthors (2004), An hourly assimilation/forecast cycle: The RUC, *Mon. Wea. Rev.*, **132**, 495-518.
- Chen, Y., S. Sun-Mack, P. Minnis, D. F. Young, and W. L. Smith, Jr., 2004: Seasonal surface spectral emissivity derived from Terra MODIS data. *Proc. 13th AMS Conf. Satellite Oceanogr. and Meteorol.*, Norfolk, VA, Sept. 20-24, CD-ROM, P2.4.
- Chiriaco, M., H. Chepfer, P. Minnis, M. Haeffelin, S. Platnick, D. Baumgardner, P. Dubuisson, M. McGill, V. Noel, J. Pelon, D. Spangenberg, S. Sun-Mack, G. Wind, 2005: Comparison of CLIPSO-like, LaRC and MODIS Retrievals of Ice Cloud Properties over SIRTa in France and Florida during CRYSTRAL-FACE, *J. Appl. Meteorol.*, in press.
- Minnis, P., L. Nguyen, W. L. Smith, Jr., M. M. Khaiyer, R. Palikonda, D. A. Spangenberg, D. R. Doelling, D. Phan, G. D. Nowicki, P. W. Heck, and C. Wolff, 2004: Real-time cloud, radiation, and aircraft icing parameters from GOES over the USA. *Proc. 13th AMS Conf. Satellite Oceanogr. and Meteorol.*, Norfolk, VA, Sept. 20-24, CD-ROM, P7.1.

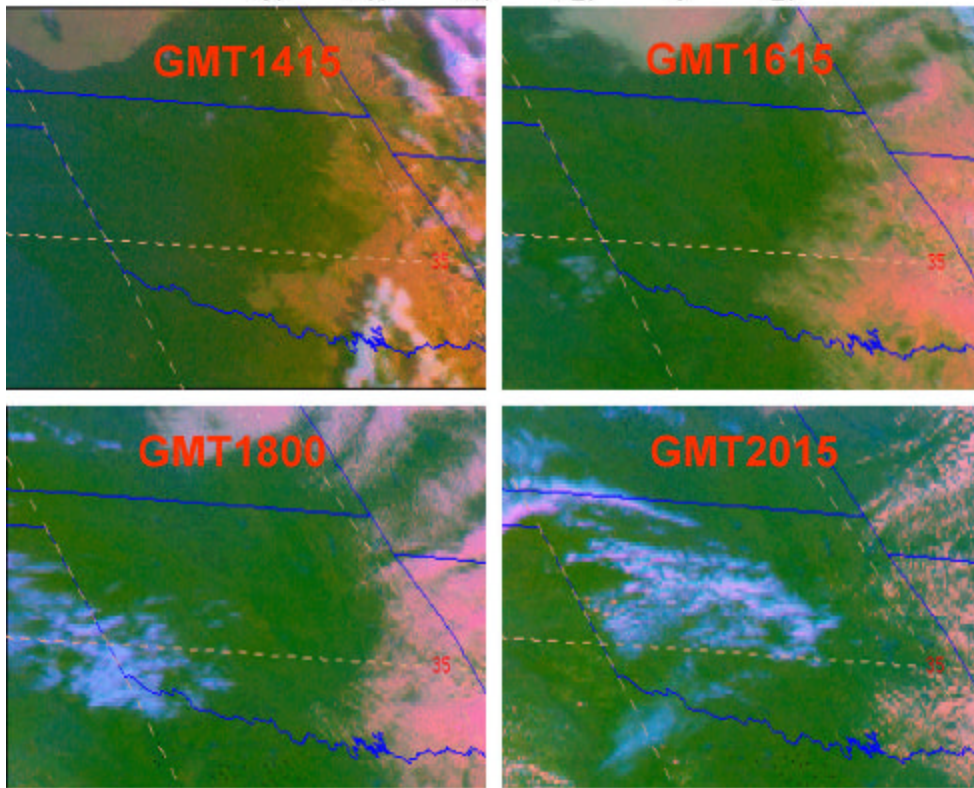
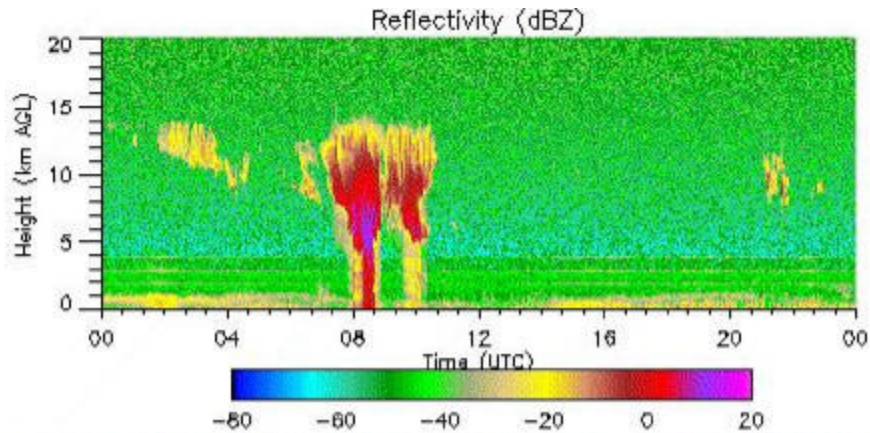


Fig. 13. Top: MMCR reflectivity. Bottom: GOES-10 RGB imagery at 1415, 1615, 1800, and 2015 UTC corresponding to the green vertical lines in Fig. 12.

Pavolonis, M. A.K. Heidinger, 2005: Preliminary Global Cloud Comparisons from the AVHRR, MODIS, and GLAS: Cloud Amount and Cloud Overlap.

Sun-Mack, S., Y. Chen, R. F. Arduini, and P. Minnis, 2004: Clear-sky narrowband albedo variations from VIRS and MODIS data. *Proc. 13th AMS Conf. Satellite Oceanogr. and Meteorol.*, Norfolk, VA, Sept. 20-24, CD-ROM, P6.34.

Trepte, Q., Y. Chen, S. Sun-Mack, P. Minnis, D.F. Young, B.A. Baum, and P. W. Heck, 1999: Scene

Identification for the CERES Cloud Analysis Subsystem, *Proc. AMS 10th Conf. Atmos. Rad.*, Madison, WI, June 28 - July 2, 169-172.

Trepte, Q., P. Minnis, and R. F. Arduini, 2002: Daytime and nighttime polar cloud and snow identification using MODIS data. *Proc. SPIE 3rd Intl. Asia-Pacific Environ. Remote Sensing Symp. 2002: Remote Sens. of Atmosphere, Ocean, Environment, and Space*, Hangzhou, China, October 23-27, Vol. 4891, 449-459.